MODELING AND ANALYSIS OF A SIX-PHASE INDUCTION GENERATOR FOR WIND ENERGY CONVERSION SYSTEMS (WECS)

LAID KHETTACHE[(1)], RACHID ABDESSEMED[(2)], ABDELHAMID BENAKCHA[(1)]

[(1)] Department of Electrical Engineering, University of Biskra – Algeria

[(2)] LEB, Department of Electrical Engineering, University of Batna – Algeria

Khettache_laid@yahoo.fr

ABSTRACT

In recent years, accumulation time and Maximum power extraction are two essential factors contributing to the development of generators. In this paper, we investigate the behavior of a model of six-phase induction generator based double-cage rotor, and compare it with that of the single cage. Initially, the proposed model was implemented in d-q reference frame, and the effect of cross saturation and excitation capacitors sizing is also incorporated in the both models to ensure the excitation process. Moreover, a detailed analysis under resistive-inductive load and constant speed drive has been carried out to assess the performance of both six-phase induction generators (single/double cage). Accurate simulation results obtained from Matlab/Simulink are used to verify and validate the effectiveness of the proposed model.

KEYWORDS: Six phase induction generator (SPIG), single cage (SC), double cage (DC), self-excited, main flux saturation, wind energy.

1 INTRODUCTION

In recent years, wind power has shown a great ability to handle increasing of load demand, scarcity of fossil fuel and greenhouse gasses effect [1]. However, the research and development of generator take important part in wind turbine system. It can be classified and cited by : 1) fixed-speed squirrel-cage induction generator; 2) doubly fed induction generator based on a power electronic converter among the grid and its rotor windings; and 3) synchronous generator,4) six- phase induction generator [2-5]. Among these generators involved, six phases induction generators (SPIG) consists of a stator with two three-phase windings identical sets that spatially shifted by an electrical angle of 30 degrees and a squirrel cage rotor [6]. It is specifically developed to be used in wind energy applications, particularly, in isolated energy generation because of the many advantages: good energy efficiency, variability of operations (Fixed and Variable Speed), reduction of the harmonic currents of the rotor and power segmentation. It is well known that a six phase induction generator can be operate in standalone mode (off-grid), but the disadvantage here is that the generator requires additional capacitors connected to its windings for self-excitation as in figure (1). Whereas the self-excited process depends entirely on the shape of its magnetization curve and that it would be impossible to analyze correctly without the non-linearity associated with the main flux saturation. For this, the phenomenon of saturation must be taken into account in our study devoted to the analysis of the SPIG self-excited [7].

Nowadays, the manufacture of induction generator has attracted significant progress in industrial development. There are four types of rotor in induction machines as per NEMA standards: i) class-A, ii) class-B, iii) class-C and, iv) class-D. Class-C design (double cage) is the most widely used type for its superior torque-slip characteristic [8], higher starting torque with a low starting current. Because of numerous advantageous features of double cage generator, this study is devoted to a modeling of the six phase induction generator with double cage rotor (SPIG-DC). In stationary reference frame, this proposed model was suggested for investigating the stability and the effect of adding capacitor in its stability and has been studied. However, in this paper we intend to show that if a squirrel double-cage six phase induction generator with the same ratings is used instead of a squirrel single-cage one (SPIG-SC), transients are reduced significantly,[9]. Initially, we analyze this procedure with modal analysis and then we will simulate it using Matlab/Simulink model. Finally, this paper is composed of seven sections. The description of the proposed generator (six- phase induction generator) is introduced in section II. Model of SPIG in d-q reference taking into account the effect of the magnetic circuit saturation is presented in section III. Section IV investigates the model of six - phase induction generator based double cage rotor (SPIG-DC). The mathematical model of resistive-inductive load connected to SPIG is implemented in section V. A comparative simulation results under

SIMULINK / MATLAB between SPIG double cage model and single cage is discussed in section VI, and the conclusion is presented in the last section.

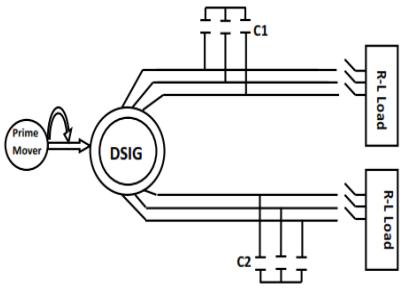

Figure 01: Representative scheme of self-excitation SPIG

2 SIX-PHASE INDUCTION GENERATOR DESCRIPTION

The six - phase induction machine (or dual star induction machine) consists of a stator carrying two identical three-phase windings but displaced each other by an angle α and a rotor which can be wound or with a squirrel cage. Each phase is represented by the equivalent diametrical winding comprising Ns turns for the stator and Nr turns for the rotor. The three coils formed the stator bundles A_{s1}, B_{s1}, C_{s1} and A_{s2}, B_{s2}, C_{s2}. The first three-phase windings called "stator 1", and the other stator bundles formed the "stator 2", where the two three-phase stator windings are spatially displaced with the angle α. On the other hand, the rotor of this machine is constituted so as to obtain three windings having a number of poles identical to that of the stator A_r, B_r, C_r figure (2).

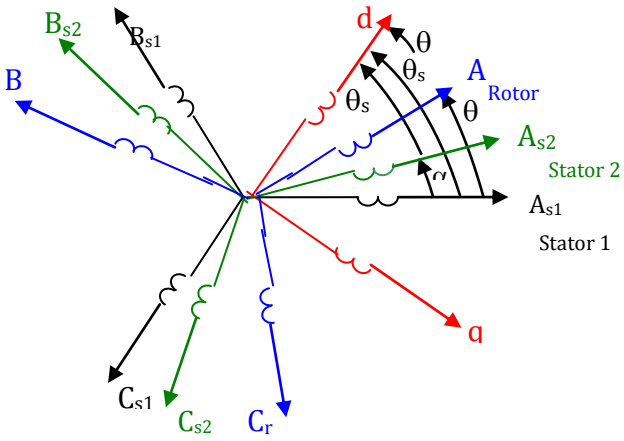

Figure 02: Representation of the stator and the rotor windings of SPIG

3 MODEL OF SIX PHASE INDUCTION GENERATOR SINGLE CAGE (SPIG-SC)

In the analysis of the transient performance of generator, the mathematical model of the six phase induction generator is defined in a synchronous reference frame. It is quite similar to that of an induction generator. Thus, the SPIG model expressed in the synchronous reference frame is decomposed into two main sub-models for the stator side and one sub-model for the rotor side as shown in Fig. 3, [10].

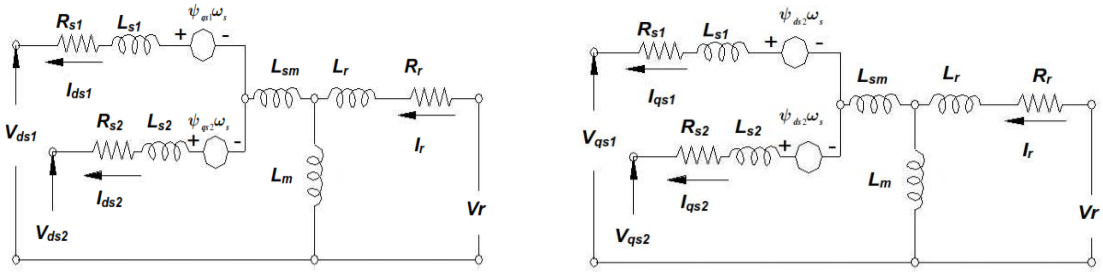

d- axis *q- axis*

Figure 03: Equivalent scheme of SPIG with single cage in d-q reference frame

3.1 Voltage equations

The dynamic voltage equations of the SPIG in the synchronous d-q reference frame are given by

$$\begin{cases} V_{ds1} = -r_1 i_{ds1} + \dfrac{d\psi_{ds1}}{dt} - \psi_{qs1}\omega_s \\ V_{qs1} = -r_1 i_{qs1} + \dfrac{d\psi_{qs1}}{dt} + \psi_{ds1}\omega_s \\ V_{ds2} = -r_2 i_{ds2} + \dfrac{d\psi_{ds2}}{dt} - \psi_{qs2}\omega_s \\ V_{qs2} = -r_2 i_{qs2} + \dfrac{d\psi_{qs2}}{dt} + \psi_{ds2}\omega_s \\ V_{dr} = 0 = r_r i_{dr} + \dfrac{d\psi_{dr}}{dt} - \psi_{qr}(\omega_s - \omega_r) \\ V_{qr} = 0 = r_r i_{qr} + \dfrac{d\psi_{qr}}{dt} + \psi_{dr}(\omega_s - \omega_r) \end{cases} \quad (1)$$

3.2 Stator and rotor flux equations

The expressions of stator and rotor fluxes are given by:

$$\begin{cases} \psi_{ds1} = -L_{s1} i_{ds1} - L_{sm}(i_{ds1} + i_{ds2}) + L_m(-i_{ds1} - i_{ds2} + i_{dr}) \\ \psi_{qs1} = -L_{s1} i_{qs1} - L_{sm}(i_{qs1} + i_{qs2}) + L_m(-i_{qs1} - i_{qs2} + i_{qr}) \\ \psi_{ds2} = -L_{s2} i_{ds2} - L_{sm}(i_{ds1} + i_{ds2}) + L_m(-i_{ds1} - i_{ds2} + i_{dr}) \\ \psi_{qs2} = -L_{s2} i_{qs2} - L_{sm}(i_{qs1} + i_{qs2}) + L_m(-i_{qs1} - i_{qs2} + i_{qr}) \\ \psi_{dr} = -L_r i_{dr} + L_m(-i_{ds1} - i_{ds2} + i_{dr}) \\ \psi_{qr} = -L_r i_{qr} + L_m(-i_{qs1} - i_{qs2} + i_{qr}) \end{cases} \quad (2)$$

With

$$\begin{cases} \psi_{md} = L_m(-i_{ds1} - i_{ds2} + i_{dr}) \\ \psi_{mq} = L_m(-i_{qs1} - i_{qs2} + i_{qr}) \\ i_{md} = -i_{ds1} - i_{ds2} + i_{dr} \\ i_{mq} = -i_{qs1} - i_{qs2} + i_{qr} \end{cases} \quad (3)$$

And the magnetizing flux ψ_m is the sum of the ψ_{md} *and* ψ_{mq}, hence:

$$\psi_m = \sqrt{{\psi_{md}}^2 + {\psi_{mq}}^2} \quad (4)$$

The cyclic saturation inductances are given by:

$$\begin{cases} L_{md} = L_m + \dfrac{i_{md}}{i_{mq}} L_{dq} = L\cos^2\delta + L_m \sin^2\delta \\ L_{mq} = L_m + \dfrac{i_{mq}}{i_{md}} L_{dq} = L\sin^2\delta + L_m \cos^2\delta \end{cases} \quad (5)$$

with:

$$\begin{cases} \cos\delta = \dfrac{i_{md}}{|i_m|} = \dfrac{\psi_{md}}{|\psi_m|} \\ \sin\delta = \dfrac{i_{mq}}{|i_m|} = \dfrac{\psi_{md}}{|\psi_m|} \end{cases} \quad (6)$$

And δ is the angle between the d axis of the common reference frame and the magnetizing current (ψ_m) space vector, where the real and imaginary components of these latter are given by i_{md} and i_{mq} (ψ_{md} and ψ_{mq}), respectively, [11].

The temporal derivatives of the magnetizing flux components can be written as:

$$\begin{cases} \dfrac{d\psi_{md}}{dt} = \dfrac{d(\psi_m \cos\delta)}{dt} = \cos\delta \dfrac{d\psi_m}{dt} - \psi_m \sin\delta \dfrac{d\delta}{dt} \\ \qquad = L\dfrac{di_{md}}{dt} + \left(i_{mq}L - \psi_m \sin\delta\right)\dfrac{d\delta}{dt} \\ \dfrac{d\psi_{mq}}{dt} = \dfrac{d(\psi_m \sin\delta)}{dt} = \sin\delta \dfrac{d\psi_m}{dt} + \psi_m \cos\delta \dfrac{d\delta}{dt} \\ \qquad = L\dfrac{di_{mq}}{dt} + \left(\psi_m \cos\delta - i_{mq}\dfrac{\cos\delta}{\sin\delta}\right)\dfrac{d\delta}{dt} \end{cases} \quad (7)$$

Where:

$$\begin{cases} \dfrac{d\psi_{md}}{dt} = L_d \dfrac{di_{md}}{dt} + L_{dq}\dfrac{di_{mq}}{dt} \\ \dfrac{d\psi_{mq}}{dt} = L_{dq}\dfrac{di_{md}}{dt} + L_q \dfrac{di_{mq}}{dt} \end{cases} \quad (8)$$

And

$$\begin{cases} L_d = L_m + \cos^2\delta\left(L - L_m\right) \\ L_q = L_m + \sin^2\delta\left(L - L_m\right) \\ L_{dq} = \cos\delta\sin\delta\left(L - L_m\right) \end{cases} \quad (9)$$

The cyclic inductance of intersaturation in the reference d-q is given by:

$$L_{dq} = \frac{i_{md}\, i_{mq}}{|\overline{i_m}|} \frac{dL_m}{d|\overline{i_m}|} = \frac{i_{md}\, i_{mq}}{|\overline{i_m}|^2}(L - L_m) \quad (10)$$

The dynamic magnetization inductances (L, L_m) are given by the following relations:

$$\begin{cases} L = \dfrac{d\left|\overline{\psi_m}\right|}{d\left|\overline{i_m}\right|} \\ L_m = \dfrac{\left|\overline{\psi_m}\right|}{\left|\overline{i_m}\right|} \end{cases} \quad (11)$$

The expression of the magnetization current is expressed by:

$$i_m = \sqrt{(-i_{ds1} - i_{ds2} + i_{dr})^2 + (-i_{qs1} - i_{qs2} + i_{qr})^2} \quad (12)$$

After deriving the system (1) by introducing the equations 2, 3 and 8, we can obtain the following system:

$$\begin{cases} -(L_{s1}+L_{sm})\dfrac{dI_{ds1}}{dt} - L_{sm}\dfrac{dI_{ds2}}{dt} + L_d\dfrac{dI_{md}}{dt} + L_{dq}\dfrac{dI_{mq}}{dt} = V_{ds1} - R_{s1}I_{ds1} + \omega_s\left((L_{s1}+L_{sm})I_{qs1} + L_{sm}I_{qs2} + \psi_{mq}\right) \\ -(L_{s1}+L_{sm})\dfrac{dI_{qs1}}{dt} - L_{sm}\dfrac{dI_{qs2}}{dt} + L_q\dfrac{dI_{mq}}{dt} + L_{dq}\dfrac{dI_{md}}{dt} = V_{qs1} - R_{s1}I_{qs1} - \omega_s\left((L_{s1}+L_{sm})I_{ds1} + L_{sm}I_{ds2} + \psi_{md}\right) \\ -(L_{s2}+L_{sm})\dfrac{dI_{ds2}}{dt} - L_{sm}\dfrac{dI_{ds1}}{dt} + L_d\dfrac{dI_{md}}{dt} + L_{dq}\dfrac{dI_{mq}}{dt} = V_{ds2} - R_{s2}I_{ds2} + \omega_s\left((L_{s2}+L_{sm})I_{qs2} + L_{sm}I_{qs1} + \psi_{mq}\right) \\ -(L_{s2}+L_{sm})\dfrac{dI_{qs2}}{dt} - L_{sm}\dfrac{dI_{qs1}}{dt} + L_q\dfrac{dI_{mq}}{dt} + L_{dq}\dfrac{dI_{md}}{dt} = V_{qs2} - R_{s2}I_{qs2} - \omega_s\left((L_s+L_{sm})I_{ds2} + L_{sm}I_{ds1} + \psi_{md}\right) \\ L_r\dfrac{dI_{dr}}{dt} + L_d\dfrac{dI_{md}}{dt} + L_{dq}\dfrac{dI_{mq}}{dt} = -R_rI_{dr} + (\omega_s - \omega_r)(L_rI_{qr} + \psi_{mq}) \\ L_r\dfrac{dI_{qr}}{dt} + L_q\dfrac{dI_{mq}}{dt} + L_{dq}\dfrac{dI_{md}}{dt} = -R_rI_{qr} - (\omega_s - \omega_r)(L_rI_{dr} + \psi_{md}) \end{cases} \quad (13)$$

3.3 Torque equations

The relation of the electromagnetic torque in generator is given by:

$$T_g = \frac{3}{2}PL_m\left[(i_{qs1} + i_{qs2})i_{dr} - (i_{ds1} + i_{ds2})i_{qr}\right] \quad (14)$$

We can write:

$$\begin{cases} \mathrm{i_{dr}} = \dfrac{\psi_{dr}}{\mathrm{L}_m + \mathrm{L}_r} + \dfrac{\mathrm{L}_m}{\mathrm{L}_m + \mathrm{L}_r}(i_{ds1} + i_{ds2}) \\ \mathrm{i_{qr}} = \dfrac{\psi_{qr}}{\mathrm{L}_m + \mathrm{L}_r} + \dfrac{\mathrm{L}_m}{\mathrm{L}_m + \mathrm{L}_r}\left(i_{qs1} + i_{qs2}\right) \end{cases} \quad (15)$$

By introducing equation (15) in (14), the final mathematical description of generator torque can be written as:

$$T_g = \frac{3}{2}P\frac{L_m}{L_r + L_m}\left[(i_{qs1} + i_{qs2})\psi_{dr} - (i_{ds1} + i_{ds2})\psi_{qr}\right] \quad (16)$$

For the considered model, we will assume that the stiffness and damping are neglected. So, the mechanical equation can be described by:

$$\begin{cases} T_g - T_m = J\dfrac{d\Omega}{dt} \\ and \\ \omega_r = p.\Omega \end{cases} \quad (17)$$

Where: Tm the torque of prime mover, and p is the number of pair poles.

3.4 Modeling of Excitation Capacitance

The modeling of the self-excitation for SPIG is summarized by the equations of the voltages at the terminals of the capacitors (C1, C2) represented in the Park reference frame as follows, [12]:

$$\begin{cases} \dfrac{d}{dt}V_{ds1} = \dfrac{1}{C_1}i_{dc1} + \omega_sV_{qs1} \\ \dfrac{d}{dt}V_{qs1} = \dfrac{1}{C_1}i_{qc1} - \omega_sV_{ds1} \\ \dfrac{d}{dt}V_{ds2} = \dfrac{1}{C_2}i_{dc2} + \omega_sV_{qs2} \\ \dfrac{d}{dt}V_{qs2} = \dfrac{1}{C_2}i_{qc2} - \omega_sV_{ds2} \end{cases} \quad (18)$$

Where I_{dc1}, I_{qc1}, I_{dc2} and I_{qc2} are the current components flowing through the excitation capacitor C_1 andC_2 connected at the terminals of stator winding sets 1 and 2, respectively.

3.5 Evaluation of Magnetizing Characteristic

The magnetic saturation phenomenon becomes a necessary condition to study an autonomous because the linear model is not able to describe the behavior of the system. Thus, this effect is not easy to simulate only, therefore we adopt a magnetic circuit which is defined by a magnetization curve obtained by experimentation and approximated by a polynomial interpolation. For considered model, the

saturation effect is taken into account by the expression of the dynamic and static magnetic inductance with respect to the magnetizing current, and can be approximated by the following polynomial interpolation, [13]:

$$\begin{cases} L_m = a_1 + a_2 i_m + a_3 {i_m}^2 + a_4 {i_m}^3 \\ L = 0.0014 - 0.0024 i_m + 0.00015 {i_m}^2 \end{cases} \quad (19)$$

Where, a_1, a_2, a_3, a_4 are constant and given in Appendix-I.

The variations of the magnetizing inductance L_m and of the dynamic inductance L as a function of the magnetization current $|I_m|$ are shown in figures 4 and 5.

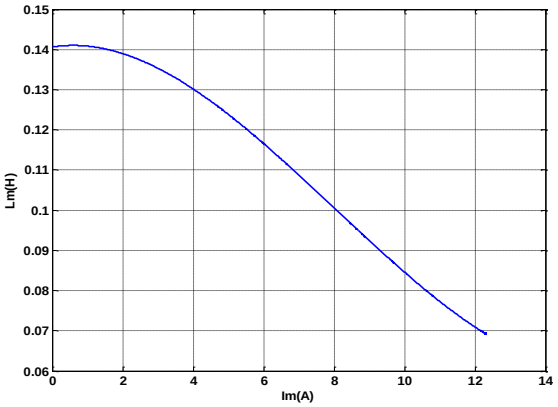

Fig.ure 04: Approximation of the magnetization inductance curve $L_m = f(i_m)$

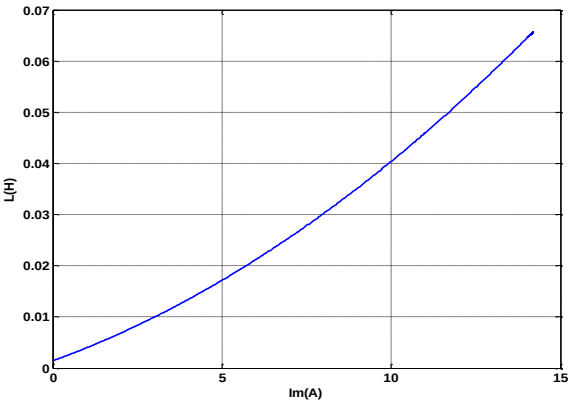

Figure 05: Evolution of dynamic inductance $L = f(i_m)$

3.6 Model of six phase induction generator with double cage rotor (SPIG-DC)

The mathematical model of a SPIG based double-cage rotor is implemented in a manner which is closely similar to the derivation of the (d, q) model of a single-cage, [14],[15]. Based on the equivalent circuit of a SPIG with double-cage shown in figure 6, the model of SPIG-DC is described by four differential equations using the common d-q reference frame. [16], [6].

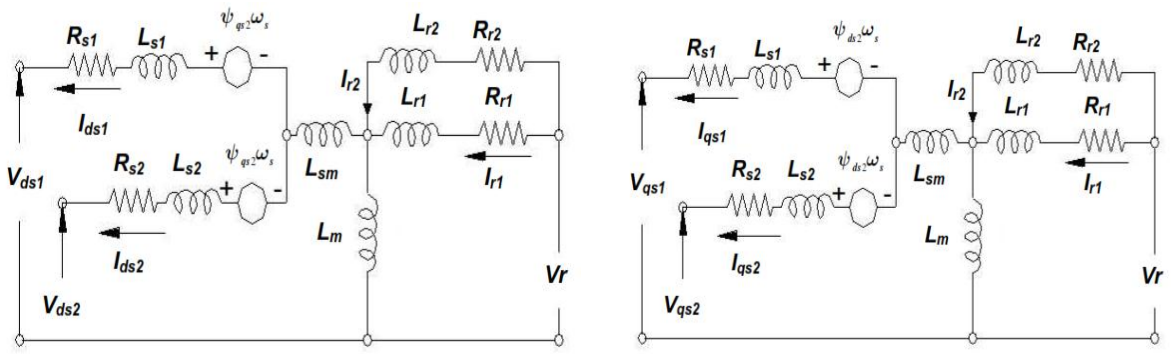

d- axis ***q- axis***

Fig.ure 06: Equivalent circuit of SPIG-DC

Adopting various assumptions of the generalized theory of electrical machines, the detailed voltage and flux equations are given below:

$$\begin{cases} V_{ds1} = -r_1 i_{ds1} + \dfrac{d\psi_{ds1}}{dt} - \psi_{qs1}\omega_s \\ V_{qs1} = -r_1 i_{qs1} + \dfrac{d\psi_{qs1}}{dt} + \psi_{ds1}\omega_s \\ V_{ds2} = -r_2 i_{ds2} + \dfrac{d\psi_{ds2}}{dt} - \psi_{qs2}\omega_s \\ V_{qs2} = -r_2 i_{qs2} + \dfrac{d\psi_{qs2}}{dt} + \psi_{ds2}\omega_s \\ V_{dr1} = 0 = r_{r1} i_{dr1} + \dfrac{d\psi_{dr1}}{dt} - \psi_{qr1}(\omega_s - \omega_r) \\ V_{qr1} = 0 = r_{r1} i_{qr1} + \dfrac{d\psi_{qr1}}{dt} + \psi_{dr1}(\omega_s - \omega_r) \\ V_{dr2} = 0 = r_{r2} i_{dr2} + \dfrac{d\psi_{dr2}}{dt} - \psi_{qr2}(\omega_s - \omega_r) \\ V_{qr2} = 0 = r_{r2} i_{qr2} + \dfrac{d\psi_{qr2}}{dt} + \psi_{dr2}(\omega_s - \omega_r) \end{cases} \quad (20)$$

Where:

r_{r1}, r_{r2} are rotor resistance of the inner and outer cage respectively;

V_{dr1}, V_{qr1}, i_{dr1}, and i_{qr1} are the rotor voltages and currents of the inner cage, respectively;

V_{dr2}, V_{qr2}, i_{dr2}, and i_{qr2} are the rotor voltages and currents of the outer cage, respectively;

In terms of simplifying the model, it is assumed that the mutual inductance between the inner and outer cage are neglected;

For this, the flux expression is described as follows:

$$\begin{cases} \psi_{ds1} = -L_{s1} i_{ds1} - L_{sm}(i_{ds1} + i_{ds2}) + L_m(-i_{ds1} - i_{ds2} + i_{dr1} + i_{dr2}) \\ \psi_{qs1} = -L_{s1} i_{qs1} - L_{sm}(i_{qs1} + i_{qs2}) + L_m(-i_{qs1} - i_{qs2} + i_{qr1} + i_{qr2}) \\ \psi_{ds2} = -L_{s2} i_{ds2} - L_{sm}(i_{ds1} + i_{ds2}) + L_m(-i_{ds1} - i_{ds2} + i_{dr1} + i_{dr2}) \\ \psi_{qs2} = -L_{s2} i_{qs2} - L_{sm}(i_{qs1} + i_{qs2}) + L_m(-i_{qs1} - i_{qs2} + i_{qr1} + i_{qr2}) \\ \psi_{dr1} = -L_{r1} i_{dr1} + L_m(-i_{ds1} - i_{ds2} + i_{dr1} + i_{dr2}) \\ \psi_{qr1} = -L_{r1} i_{qr1} + L_m(-i_{qs1} - i_{qs2} + i_{qr1} + i_{qr2}) \\ \psi_{dr2} = -L_{r2} i_{dr2} + L_m(-i_{ds1} - i_{ds2} + i_{dr1} + i_{dr2}) \\ \psi_{qr2} = -L_{r2} i_{qr2} + L_m(-i_{qs1} - i_{qs2} + i_{qr1} + i_{qr2}) \end{cases} \quad (21)$$

Where:

L_{r1}: Rotor leakage inductance of the inner cage;

L_{r2} : Rotor leakage inductance of the outer cage;

L_{sm} is the common mutual leakage inductance between the stators windings 1 and 2; L_s and L_r are the stator and the rotor leakage inductance respectively, and L_m is the magnetizing inductance between the stator and the rotor.

The magnetizing current and magnetizing flux d,q-axis components are :

$$\begin{cases} \psi_{md} = L_m(-i_{ds1} - i_{ds2} + i_{dr1} + i_{dr2}) \\ \psi_{mq} = L_m(-i_{qs1} - i_{qs2} + i_{qr1} + i_{qr2}) \\ i_{md} = -i_{ds1} - i_{ds2} + i_{dr1} + i_{dr2} \\ i_{mq} = -i_{qs1} - i_{qs2} + i_{qr1} + i_{qr2} \end{cases} \quad (22)$$

Introducing the relations between the flux links and currents equations 21, 22 into voltages equations 20, the final equations of the proposed model are expressed as follows:

$$\begin{cases} -(L_{s1} + L_{sm})\dfrac{dI_{ds1}}{dt} - L_{sm}\dfrac{dI_{ds2}}{dt} + L_d\dfrac{dI_{md}}{dt} + L_{dq}\dfrac{dI_{mq}}{dt} = V_{ds1} - R_{s1}I_{ds1} + \omega_s\left((L_{s1} + L_{sm})I_{qs1} + L_{sm}I_{qs2} + \psi_{mq}\right) \\ -(L_{s1} + L_{sm})\dfrac{dI_{qs1}}{dt} - L_{sm}\dfrac{dI_{qs2}}{dt} + L_q\dfrac{dI_{mq}}{dt} + L_{dq}\dfrac{dI_{md}}{dt} = V_{qs1} - R_{s1}I_{qs1} - \omega_s\left((L_{s1} + L_{sm})I_{ds1} + L_{sm}I_{ds2} + \psi_{md}\right) \\ -(L_{s2} + L_{sm})\dfrac{dI_{ds2}}{dt} - L_{sm}\dfrac{dI_{ds1}}{dt} + L_d\dfrac{dI_{md}}{dt} + L_{dq}\dfrac{dI_{mq}}{dt} = V_{ds2} - R_{s2}I_{ds2} + \omega_s\left((L_{s2} + L_{sm})I_{qs2} + L_{sm}I_{qs1} + \psi_{mq}\right) \\ -(L_{s2} + L_{sm})\dfrac{dI_{qs2}}{dt} - L_{sm}\dfrac{dI_{qs1}}{dt} + L_q\dfrac{dI_{mq}}{dt} + L_{dq}\dfrac{dI_{md}}{dt} = V_{qs2} - R_{s2}I_{qs2} - \omega_s\left((L_s + L_{sm})I_{ds2} + L_{sm}I_{ds1} + \psi_{md}\right) \\ L_{r1}\dfrac{dI_{dr1}}{dt} + L_d\dfrac{dI_{md}}{dt} + L_{dq}\dfrac{dI_{mq}}{dt} = -R_{r1}I_{dr1} + (\omega_s - \omega_r)(L_{r1}I_{qr1} + \psi_{mq}) \\ L_{r1}\dfrac{dI_{qr1}}{dt} + L_q\dfrac{dI_{mq}}{dt} + L_{dq}\dfrac{dI_{md}}{dt} = -R_{r1}I_{qr1} - (\omega_s - \omega_r)(L_{r1}I_{dr1} + \psi_{md}) \\ L_{r2}\dfrac{dI_{dr2}}{dt} + L_d\dfrac{dI_{md}}{dt} + L_{dq}\dfrac{dI_{mq}}{dt} = -R_{r2}I_{dr2} + (\omega_s - \omega_r)(L_{r2}I_{qr2} + \psi_{mq}) \\ L_{r2}\dfrac{dI_{qr2}}{dt} + L_q\dfrac{dI_{mq}}{dt} + L_{dq}\dfrac{dI_{md}}{dt} = -R_{r2}I_{qr2} - (\omega_s - \omega_r)(L_{r2}I_{dr2} + \psi_{md}) \end{cases} \quad (23)$$

In similarly of previous part, the expressions for electromagnetic torque of SPIG-DC can be expressed as:

$$T_{gdouble} = \frac{3}{2} p((\psi_{ds1} i_{qs1}) + (\psi_{ds2} i_{qs2}) - (\psi_{qs1} i_{ds1}) - (\psi_{qs2} i_{ds2})) \quad (24)$$

Where, the relations between generator torque and currents components are:

$$T_{gdouble} = \frac{3}{2} p L_m ((i_{qs1} + i_{qs2}).(i_{dr1} + i_{dr2}) - (i_{ds1} + i_{ds2}).(i_{qr1} + i_{qr2})) \quad (25)$$

The active and reactive powers in stator windings '1'are:

$$\begin{cases} P_{s1} = V_{ds1} i_{ds1} + V_{qs1} i_{qs1} \\ Q_{s1} = V_{qs1} i_{ds1} - V_{ds1} i_{qs1} \end{cases} \quad (26)$$

3.7 SPIG (single/double cage) with R-L load

In this section, the both stator windings of the machine are star-connected to a capacitance bank C=60µF, which is parallel to the resistive and inductive load (seen in Fig. 1), the equations related to these parts must be added to the generator which is driven at a constant speed 155 rad/s.

$$\begin{cases} \frac{d}{dt} V_{ds1} = \frac{1}{C_1} (i_{ds1} - i_{ds1L}) + \omega_s V_{qs1} \\ \frac{d}{dt} i_{ds1L} = \frac{1}{L} (V_{ds1} - R i_{ds1L}) + \omega_s i_{qs1L} \\ \frac{d}{dt} V_{qs1} = \frac{1}{C_1} (i_{qs1} - i_{qs1L}) - \omega_s V_{ds1} \\ \frac{d}{dt} i_{qs1L} = \frac{1}{L} (V_{qs1} - R i_{qs1L}) + \omega_s i_{ds1L} \end{cases} \quad (27)$$

$$\begin{cases} \frac{d}{dt} V_{ds2} = \frac{1}{C_2} (i_{ds2} - i_{ds2L}) + \omega_s V_{qs2} \\ \frac{d}{dt} i_{ds2L} = \frac{1}{L} (V_{ds2} - R i_{ds2L}) + \omega_s i_{qs2L} \\ \frac{d}{dt} V_{qs2} = \frac{1}{C_2} (i_{qs2} - i_{qs2L}) - \omega_s V_{ds2} \\ \frac{d}{dt} i_{qs2L} = \frac{1}{L} (V_{qs2} - R i_{qs2L}) + \omega_s i_{ds2L} \end{cases} \quad (28)$$

Where: I_{ds1L}, I_{qs1L} and I_{ds2L}, I_{qs2L} are the load current components in the synchronous d-q reference frame, respectively, and R, L are the resistive and inductive load components.

3.8 Simulation results

To demonstrate the efficiency of the proposed model (SPIG based double cage rotor), a comparison between single (solid line) and double cage (dashed line) structures using Matlab/ Simulink simulator was performed. These generators were driven at a constant speed of 155 rad/s and self-excitation capacitors equal to 60 µF.

3.9 SPIG without load test

The figures 7, 8 and 10 show the simulation results of the output voltage V_a, current phase I_a and magnetization current Im respectively.

According to these figures, an exponential form can be observed in the period t=0s and t=1.5s for the both generators, then it stabilizes at a fixed value, which finds that the evolution of the stator voltages and current follows the evolutionary form of the magnetization current. Moreover, the shift angle $\alpha = \frac{\pi}{6}$ between two currents related to each phase for each star is shown in figure (9). On the other hand, we note that the accumulation process (accumulation time tac) is much faster in about 0.22s for the double cage (tac2=0.91s) than the single cage (tac1=1.13s), with a small increase 3.64%, 3.43 % in voltage and current as shown. The electromagnetic torque, active and reactive stator power as shown in figures (11, 12) respectively, are taking the same form of the magnetization current curve. In addition, the increase in torque, active and reactive power for SPIG based double cage are observed.

3.10 SPIG with load test

The SPIG is examined under *R-L* load condition applied at t=1.5s where *R=100* Ω and *L=0.8H*. The insertion of the load gives rise to decreases in the set characteristics of the SPIG compared to those observed in no load operation, where the values are illustrated in the table below:

Table01: Output values of SPIG with single and double cage of the rotor

	Single cage	Double cage	Increase values
Va (V)	247	256	9
Ia (A)	4.66	4.82	0.16
Im(A)	11.54	11.77	0.23
Tg (N.m)	12.83	13.72	0.89
Ps (W)	162	281	119
Qs (VAR)	2586	2818	232
t_{ac} (s)	1.13	0.91	0.22

The causes of these decreases are the same as those of the conventional induction generator. The connection of a load will decrease the excitation current supplied by the capacitors, thus the large reactive energy consumption when uses inductive load. Hence, this decrease in current means less flux, which affects the magnetization of the machine.

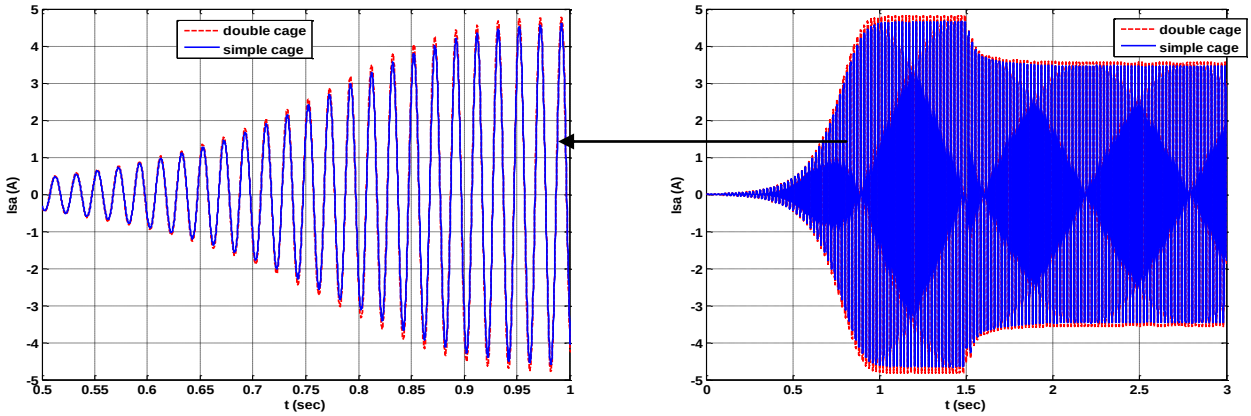

Figure 07: Comparison of output stator voltage of SPIG between single cage (solid line'-') and double cage (dashed line'- -') with self-excitation capacitance c=60µF and rotor speed w_r=155 rad/s at load condition

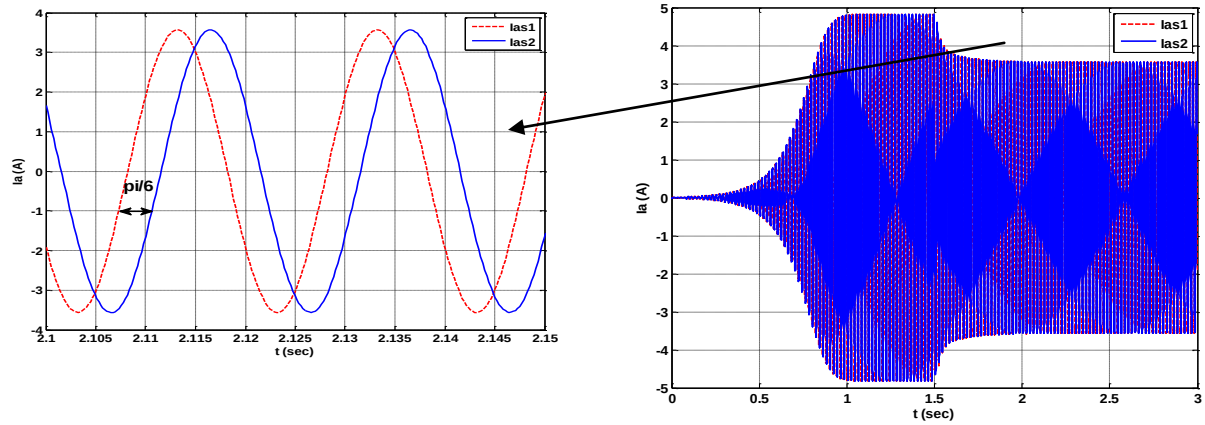

Figure 08: Stator currents phases (star1, star2) of SPIG at load condition

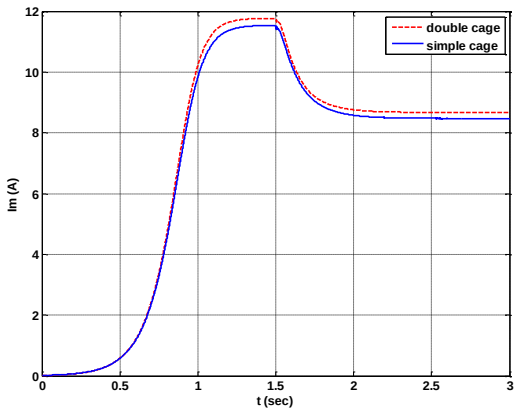

Fig.ure 09: Comparison of magnetization currents Im, single cage (solid line'-') and double cage (dashed line'- -')

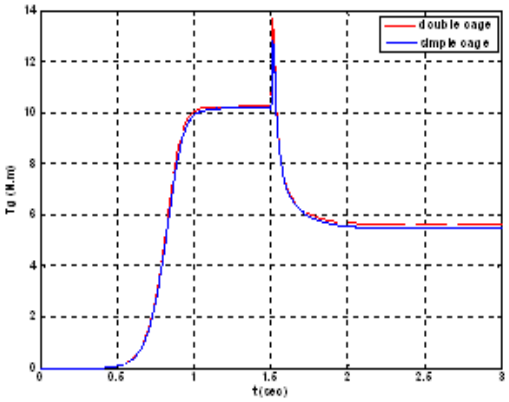

Fig.ure 11: The generated Electromagnetic torque

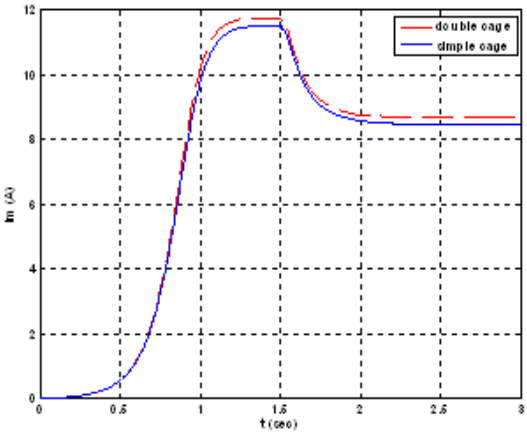

Figure 10: Comparison of magnetization currents Im, single cage (solid line'-') and double cage (dashed line'- -')

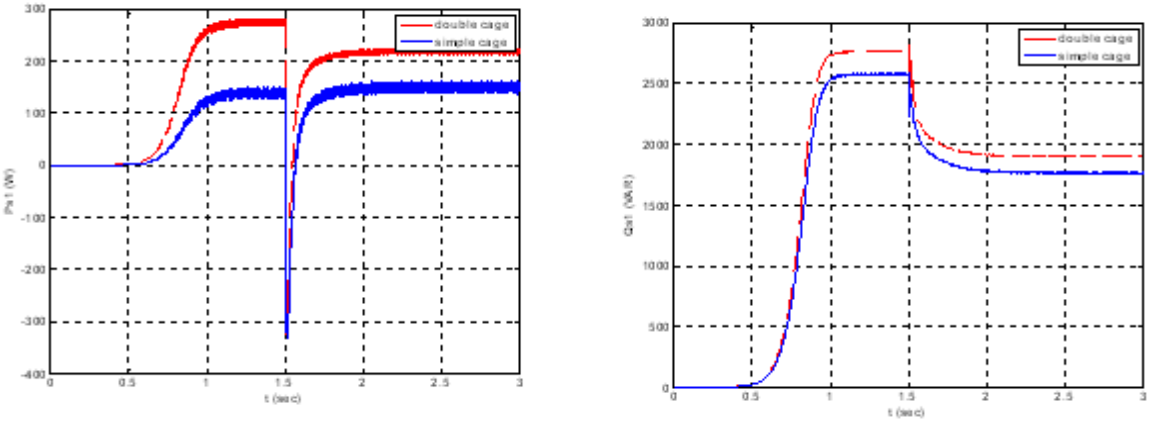

a)Active power ***b) Reactive power***

Figure 12: Representation of the generated active and reactive stator power

3.11 SPIG with critical load test

In order to investigate our approach under critical conditions, a critical load ($R = 120\ \Omega$, $L = 0.08\ H$) is applied at t = 2s to study the both generators performance. In this context, figure (13) shows the variation of the voltage as function of time. From this figure, it is clearly shown that a drop in output voltage, about 94.2%, is

recorded for SPIG double cage structure. Moreover, a degradation of 100% is observed for SPIG single cage. This result is mainly due to the short-circuit phenomenon of both generators caused by the applied critical charge as it is shown in figure (14). Also, this loading decreases the magnetizing current Im, as seen in figure (15), which results in the reduced flux.

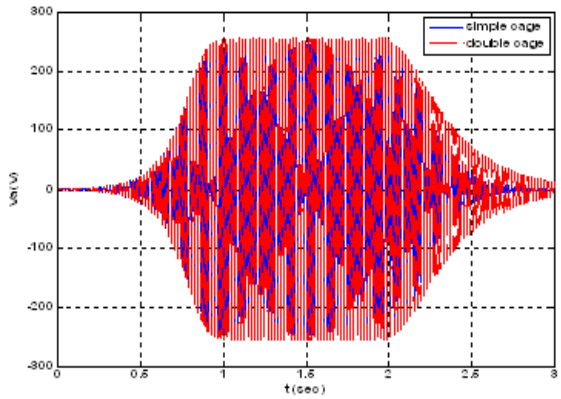

Figure 13: Comparison of output stator voltage of SPIG between single cage (solid line'-') and double cage (dashed line'- -') at critical loads

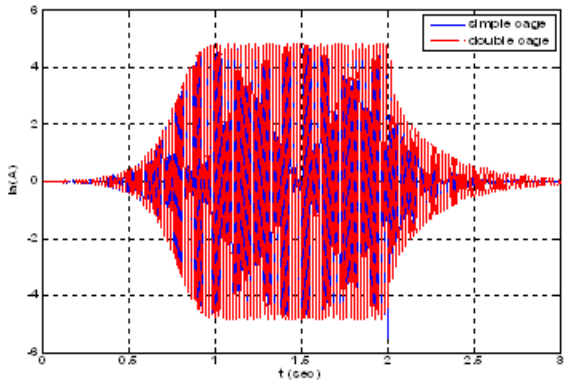

Figure 14: Comparison of stator currents phase of SPIG based (single and double cage models) at critical loads

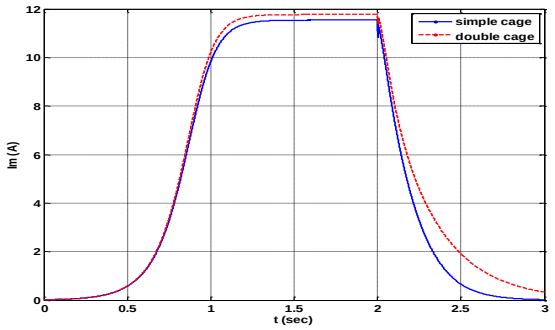

Fig.ure 15: Comparison of magnetization currents Im, single cage (solid line'-') and double cage (dashed line'- -') at critical loads

It is to note that this insignificant increasing in the output parameters is mainly due to the investigated machines, which are low power ones [13], where new results and mechanisms can be observed for high power machines. However, new simulations and models should be developed in this case by taking into account other effects and parasitic parameters.

4 CONCLUSION

This work is devoted to develop an analytical model of SPIG based double cage rotor under cross-saturation effect. The latter is taken into account through the expression of the static and dynamic magnetizing inductances with respect to the magnetizing current. Then they are evaluated from the open circuit d-axis magnetizing curve. A nonlinear mathematical model in the d-q axis of the six phase induction generator with the single and double cage was developed. In view of the obtained results and observations, the comparison between single and double cage generators shows several advantages such as:

- The double cage machine is more stable than the single cage one.
- An increase in active stator power is obtained for the double cage structure.
- The accumulation time in double cage machine (0.06s) is very short compared to the single cage one.

The proposed investigation can extended to study more complex machines. However, new complex models should be developed in this case by taken into account other effects and parasitic parameters.

APPENDIX

The parameters of the six phase induction generator used by [13] as follows:

Stator resistances: $r_{s1} = r_{s2} = 1.9\ \Omega$,

Stator inductances: $L_{s1}, = L_{s2} = 0.0132\ H$,

Single cage:

Rotor resistance $r_r = 2.12\ \Omega$,

Rotor inductance $L_r = 0.0132H$

Double cage:

Rotor resistance inner cage: $r_{r1} = 6.48\ \Omega$,

Rotor resistance outer cage: $r_{r2} = 3.12\ \Omega$,

Rotor inductance of the inner cage: $L_{r1} = 0.008\ H$

Rotor inductance of the outer cage: $L_{r2} = 0.0112\ H$

mutual inductance between stator and rotor: $L_m = 0.011\ H$

$n=1480\ tr/min$; $J=0.038\ kg.m^2$

Resistive and Inductive load:

$L_L=0.8\ H$

$R_L=100\ \Omega$

The constants in magnetization characteristics of SPIG are as:

$a_1 = 0.1406$, $a_2 = 0.0014$, $a_3 = -0.0012$, and $a_4 = 0.000050$.

REFERENCES

[1] Tan WS, Hasan MY, Majid S, Rahman HA. Optimal distributed renewable generation planning: A review of different approaches. Renewable and Sustainable Energy Reviews vol. 18; 2013, p. 626-645.

[2] Dehghanzadeh Ali Reza, Behjat Vahid, Banaei Mohamad Reza. Dynamic modeling of wind turbine based axial flux permanent magnetic synchronous generator connected to the grid with switch reduced converter. Ain Shams Eng J 2015. in press, Corrected Proof

[3] C.H. Ng, M.A. Parker, L. Ran, P.J. Tavner, J.R. Bumb y, E. Spooner. A multilevel modular converter for a large, light weight wind turbine generator. IEEE Trans Power Electron, 23 (2008), pp. 1062-1074

[4] Z. Chen, J.M. Guerrero, F. Blaabjerg. A review of the state of the art of power electronics for wind turbines. IEEE Trans. Power Electron., 24 (2009), pp. 1859-1875

[5] J.M. Carrasco, L.G. Franquelo, J.T. Bialasiewicz, E. G alvan, R.C.P. Guisado, A.M. Prats, et al. Power electronic systems for the grid integration of renewable energy sources: a survey. IEEE Trans. Industr. Electron., 53 (2006), pp. 1002-1016.

[6] Munoz AR, Lipo TA. Dual stator winding induction machine drive. IEEE Transactions on Industry Application 2000; 36:1369–1379.

[7] E. Levi and D. Rauski. Modelling of deep-bar and double-cage self-excited induction generators for wind-electricity generation studies. Electr. Power Syst. Res., vol. 27, no. 1, pp. 73–81, May 1993.

[8] S. J. Chapman. Electric machinery fundamentals. 4th Edition, Toronto: McGRAW-HILL, 2005.

[9] Mirbagheri, Seyed Mohsen, et al. The comparison of single-cage and double-cage induction generators at variable frequencies. Power Electronics, Drives and Energy Systems (PEDES), 2012 IEEE International Conference on. IEEE, 2012.

[10] Nounou, Kamel, et al. Six-phase induction machine operating as a standalone self-excited induction generator. Green Energy, 2014 International Conference on. IEEE, 2014.

[11] Levi, E. Applications of the current state space model in analyses of saturated induction machines. Electric power systems research 31.3 (1994): 203-216.

[12] Natarajan, K., Sharaf, A.M., Sivakumar, S. and Nagnarhan, S. Modeling and Control Design for Wind Energy Conversion Scheme using Self-Excited Induction Generator. IEEE Trans. On E.C., Vol. 2,No. 3,pp.506-512, Sept. 1987.

[13] Singh, G. K., K. B. Yadav, and R. P. Saini. Modeling and analysis of multi-phase (six-phase) self-excited induction generator. Electrical Machines and Systems, 2005. ICEMS 2005. Proceedings of the Eighth International Conference on. Vol. 3. IEEE, 2005.

[14] P. Kundur. Power System Stability and Control. New York: McGraw-Hill, 1994.

[15] O. Anaya-Lara, N. Jenkins, J. Ekanayake, P. Cartwright and M. Guges. Wind Energy Generation: Modeling and Control. USA: Wiley, 2009.

[16] Guru, Neelakantha, Santosh Kumar Mishra, and B. Nayak. Indirect Vector Control of Multi Cage Induction Motor. International Journal of Computer Applications 68.2 (2013).